

## SELECTION OF IDEAL FEED PROFILE FOR ASYMPTOTIC CONICAL DIPOLE FED IMPULSE RADIATING ANTENNA

Dhiraj K. Singh<sup>1, \*</sup>, Devendra C. Pande<sup>1</sup>,  
and Amithabha Bhattacharya<sup>2</sup>

<sup>1</sup>Electronics & Radar Development Establishment, Bangalore, India

<sup>2</sup>Indian Institute of Technology, Kharagpur, India

**Abstract**—Equivalent charge method is used to design ultra wide band asymptotic conical dipole (ACD) antenna. Combination of linear charge density and point charges is used to generate different profiles for ACD antennas. Two different profiles of ACD antenna are used as a feed for reflector based impulse-radiating antennas (IRAs). This paper focuses on the selection of ideal ACD profile as well as the requisite charge distribution for ACD antenna as a feed to design  $100\ \Omega$  input impedance reflector IRA. An ideal Configuration of ACD feeding structure for reflector IRA is chosen based on FDTD analysis results. To validate the utility of the proposed new feed an ACD-fed half IRA is realized with input impedance of nearly  $50\ \Omega$ . Measurements are carried out using single-ended instrumentation without any impedance adaptor as commonly done with Conventional IRAs.

### 1. INTRODUCTION

Biconical structures are known for their wideband characteristics and their different variants have been worked out in past for various antenna geometries. Reflector based ultra wideband (UWB) biconical antennas popularly known as impulse radiating antennas (IRAs) [1–6] have been developed for good directional and time domain characteristics. IRAs are commonly designed for  $200\ \Omega$  input impedance wherein the conical plate transmission line feed used is of  $400\ \Omega$ . Typically, in an IRA, two  $400\ \Omega$  conical plate lines are connected in parallel at the feed point to get  $200\ \Omega$  input impedance.

---

*Received 28 August 2012, Accepted 12 December 2012, Scheduled 13 December 2012*

\* Corresponding author: Dhiraj Kumar Singh (dhiraj.lrde@gmail.com).

The reason for choosing a  $400\ \Omega$  line is to get a smaller cone angle for the transmission line thereby reducing the aperture blockage and, in turn, achieving a better antenna gain. Most of the pulse generators have an unbalanced coaxial output with a  $50\ \Omega$  source resistance. To Connect  $50\ \Omega$  voltage source to the  $200\ \Omega$  input of IRA, a  $50\ \Omega$  to  $200\ \Omega$  balun is used. ACD fed reflector IRAs [15] shows promise to reduce the input impedance of IRAs without reduction in gain and hence exempts use of  $50\ \Omega$  to  $200\ \Omega$  balun.

This paper describes ACD antennas of different profiles generated due to different charge distributions and selection of optimum ACD profile as feed to get a  $100\ \Omega$  IRA. ACD fed IRA with two different feed profile was analyzed using FDTD and the ideal feed profile was chosen based on these results. The analysis results were validated by doing measurement on realized half IRA (HIRA) of nearly  $50\ \Omega$  input impedance. In Section 2 of the paper, the design formulas and different profiles for this ACD feed is presented. The time domain analysis of IRA with ACD feed arms with different profile is discussed in Section 3. Time domain measurement results are elaborated in Section 4. Discussion and Conclusion are presented in Sections 5 & 6 respectively.

## 2. FEEDING DIPOLE DESIGN

Equivalent charge method [9, 15] is used to generate the profile of the ACD antenna. In the equivalent charge method, a hypothetical static charge distribution is defined with the total charge set equal to zero. This distribution is defined to be rotationally symmetric about  $z$ -axis with opposite charge reflected about the symmetry plane ( $x$ - $y$  plane) as shown in Fig. 1. The derivation of potential distribution from this equivalent charge is done using cylindrical ( $r, \varphi, z$ ) coordinate systems as shown in Fig. 2. Two equipotential surfaces of equal and opposite potentials are thus generated defines the profile of the biconical antenna. Both of these surfaces can be realized by perfect electric conductors with an appropriate total surface charge such that the potential distribution external to the surface remains unchanged.

The equivalent line charge  $\lambda(z)$  and the two point charges  $Q$  on the  $z$ -axis be given by [12]:

$$\lambda(z) = \begin{cases} \lambda_0, & 0 < z < z_0 \\ -\lambda_0, & 0 > z > -z_0 \\ 0, & z = 0, z > z_0 \end{cases} \quad (1)$$

$$Q = \begin{cases} Q_0, & z = z_0 \\ -Q_0, & z = -z_0 \end{cases}$$

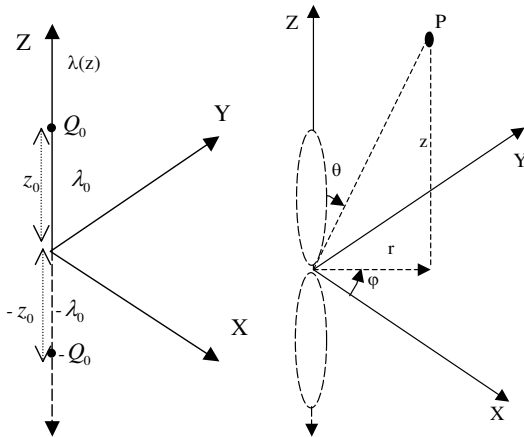


**Figure 1.** Charge distribution.

**Figure 2.** Biconical geometry.

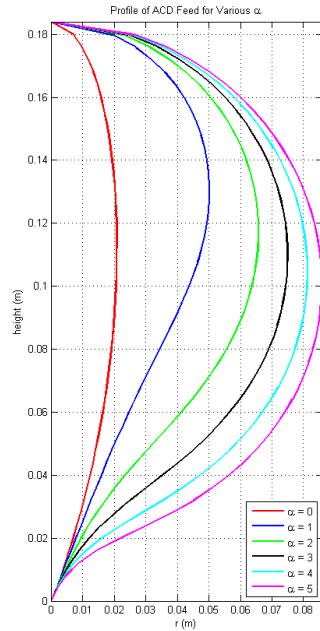


**Figure 3.** ACD Contours.

where mean charge separation  $z_0 > 0$ , charge density  $\lambda_0 > 0$ , and discrete charge  $Q_0 > 0$ .

In order to generate the ACD profile, we need to find out the ACD counter co-ordinates  $(r, z)$ . The potential distribution of this charge distribution is the superposition of the potentials from the distributed charges and the point charges. The potential function generated by the line charges is given by Eq. (2).

Potential distribution due to this equivalent charge distribution, at any point  $P(r, \varphi, z)$  in cylindrical coordinates is

$$\phi_l = \frac{\lambda_0}{4\pi\epsilon_0} \ln \left\{ \frac{[z + \sqrt{z^2 + r^2}]^2}{\left[ z + z_0 + \sqrt{(z + z_0)^2 + r^2} \right] \left[ z - z_0 + \sqrt{(z - z_0)^2 + r^2} \right]} \right\} \quad (2)$$

The potential at a point  $(z, r)$  due to the two point charges is

given by

$$\phi_p = \frac{Q_0}{4\pi\epsilon_0} \left( \frac{1}{\sqrt{(z-z_0)^2 + r^2}} - \frac{1}{\sqrt{(z+z_0)^2 + r^2}} \right) \quad (3)$$

The total charge on the positive line segment is  $\lambda_0 z_0$ . A dimensionless quantity  $\alpha$  is defined as the ratio of the point charge to the line charge, so that

$$Q_0 = \alpha \lambda_0 z_0 \quad (4)$$

The summation of potential due to line charge and point charge is equated to the surface potential of an infinite biconical structure. The two equipotential biconical Surfaces are defined as shown in Fig. 2. The surface potential function and characteristic impedance for an infinite biconical structure after simplification is given by [13]

$$\phi_s = \frac{\lambda_0}{2\pi\epsilon_0} \ln \left[ \cot \left( \frac{\phi_0}{2} \right) \right] \quad (5)$$

$$Z_c = 120 \ln (\Theta_0^{-1}) \quad (6)$$

where,  $\Theta_0 = \tan(\frac{\theta_0}{2})$ ,  $Z_c =$  Characteristic impedance of infinite bicone in free space,  $\theta_0 =$  Bicone angle.

When we equate the total potential distribution to that of the infinite bicone  $\phi_s$ , the  $(z, r)$  coordinates for the asymptotic conical profiles are given in terms of  $\Theta_0$  as

$$\ln (\Theta_0^{-2}) = \ln \left\{ \frac{[z + \sqrt{z^2 + r^2}]^2}{\left[ \frac{z+z_0 + \sqrt{(z+z_0)^2 + r^2}}{\alpha z_0} \right] \left[ \frac{z-z_0 + \sqrt{(z-z_0)^2 + r^2}}{\alpha z_0} \right]} \right\} + \frac{\alpha z_0}{\sqrt{(z-z_0)^2 + r^2}} - \frac{\alpha z_0}{\sqrt{(z+z_0)^2 + r^2}} \quad (7)$$

The antenna element height is determined by setting  $r = 0$  at  $z = h$ , which gives

$$\ln (\Theta_0^{-2}) = \ln \left( \frac{h^2}{h^2 - z_0^2} \right) + \frac{2\alpha z_0^2}{h^2 - z_0^2} \quad (8)$$

where,  $\Theta_0$  is a constant determined by the desired asymptotic impedance from the infinite biconical surface [9]. For each value of  $z$  between zero and the antenna height  $h$ , there exists a unique element radius  $r$ . For any given value of  $\Theta_0$ ,  $\alpha$ , and  $h$ , Eq. (8) is solved numerically for  $z_0$  using Newton-Raphson method. Once  $z_0$  and  $\Theta_0$  are determined for a particular configuration, Eq. (7) is solved iteratively

to get the antenna feed contour for various values of  $\alpha$ , as shown in Fig. 3. The  $200\ \Omega$  asymptotic conical dipoles for both  $\alpha = 0$  & 1 profiles are individually analyzed without any resistive termination for its return loss with respect to frequency using an excitation source impedance of  $200\ \Omega$ . A gaussian pulse of 50 ps full width half maximum (FWHM), 50 ps rise time and 0.56 volts peak amplitude as shown in Fig. 13 is used as excitation for simulation. An absorbing boundary condition with seven perfectly matched layers (PML) is used for this simulation.

The calculation of return loss is done for the solid ACD geometry (obtained by rotating the contour of Fig. 3  $360^\circ$  around the height axis) as well as the ACD plate of length 184 mm and 2 mm thickness (obtained using a surface profile shown in Fig. 3 and its mirror image) for both  $\alpha = 0$  & 1 (shown in Fig. 4). The return loss plots for the geometries for  $\alpha = 0$  and  $\alpha = 1$  are shown in Fig. 5 and Fig. 6. Both of these plots show that solid geometries of both profiles have better impedance matching performance than plates. Though the solid ACD geometry has better impedance matching than plate, still flat ACD is used in this new antenna design to reduce the feed blockage as well as weight of the antenna. The return loss plot as shown in Fig. 6 shows less wiggles for ACD solid geometry and there is a marked resonance near 4 GHz. The larger girth of the solid dipole for  $\alpha = 1$  profile reduces the inductance, hence wiggles in return loss plot is reduced. The resonance

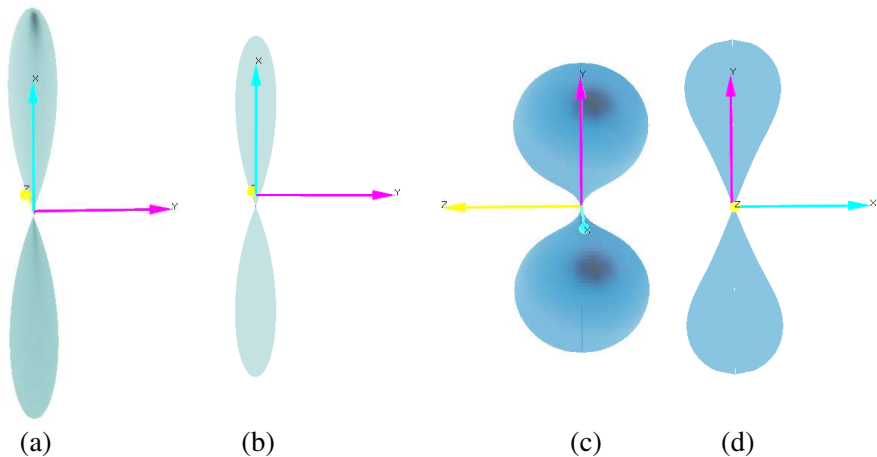


**Figure 4.** ACD geometry profile ( $\alpha = 0$  & 1). (a) ACD solid geometry ( $\alpha = 0$ ). (b) Flat ACD ( $\alpha = 0$ ). (c) ACD solid geometry ( $\alpha = 1$ ). (d) Flat ACD plate ( $\alpha = 1$ ).

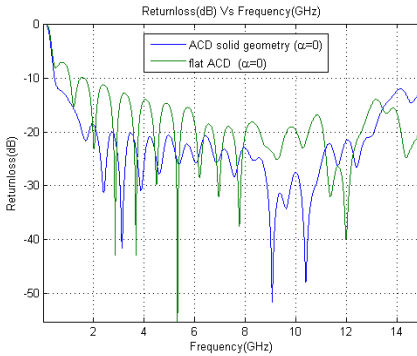


**Figure 5.** Return loss (dB) vs frequency (Hz) (simulation).

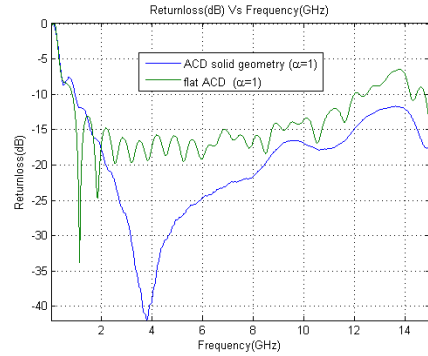


**Figure 6.** Return loss (dB) vs frequency (Hz) (simulation).

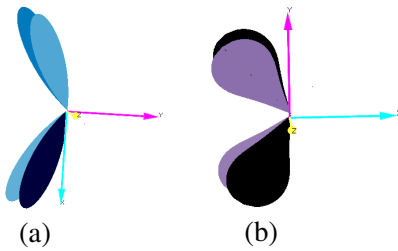


**Figure 7.** Feed arm geometry of ( $\alpha = 0$  &  $1$ ) profiles. (a) ACD feed arms ( $\alpha = 0$ ). (b) ACD feed arms ( $\alpha = 1$ ).

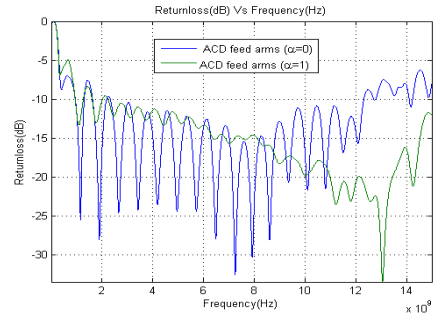


**Figure 8.** Simulated return loss of ACD feed arms ( $\alpha = 0$  &  $1$ ).

observed near 4 GHz is attributed to the charge separation between point charge and the mean linear charge.

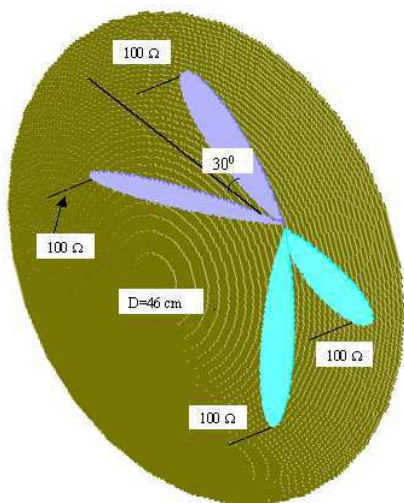
Two asymptotic conical dipole plates out of both these profiles of length 184 mm and 2 mm thickness were connected in parallel at the feed point to get an input impedance of nearly half the value of the individual dipoles. The combined arms were rotated around the feed point towards the reflector as shown in Fig. 7. The combined feed arms of both profiles are analyzed without reflector and terminating resistors, using excitation source impedance as  $100 \Omega$ . A gaussian pulse of 50 ps FWHM, 50 ps rise time and 0.56 volts peak amplitude as shown in Fig. 13 is used as excitation for simulation. An absorbing boundary

condition with seven perfectly matched layers (PML) is used for this simulation. The calculated return loss plot of the combined feed arms for both profiles is shown in Fig. 8.

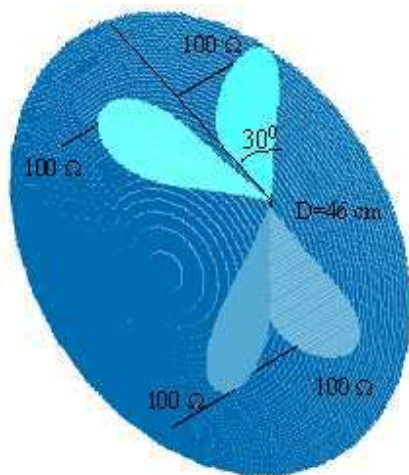
### 3. ANTENNA DESIGN AND ANALYSIS

Reflector-based IRAs are designed using a 46 cm diameter parabolic reflector with focal length 18.4 cm using the combined flat ACD feed arms of length 184 mm and 2 mm thickness of both  $\alpha = 0$  & 1 profiles as shown in Fig. 9 and Fig. 10. Two  $200\ \Omega$  asymptotic conical dipoles of both profiles connected in parallel at the input of the IRA give a  $100\ \Omega$  input impedance for the new IRA. Feed arms are placed at  $\pm 30$  degrees from the vertical axis for both feed profiles. ACD-fed IRA for both the profiles ( $\alpha = 0$  & 1) is analyzed in time domain using the finite difference time domain solver XFDTD (v7.1).

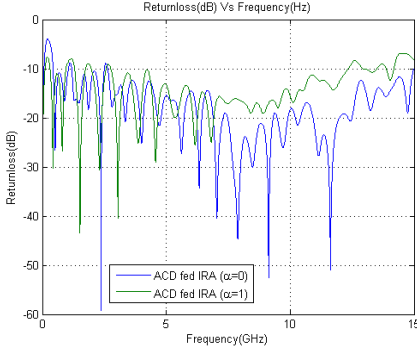
The excitation waveform used for the simulation of the antenna is a gaussian pulse of amplitude  $\sim 0.56$  volts, FWHM  $\sim 50$  ps and rise time  $\sim 50$  ps as shown in Fig. 13. The absorbing boundary condition with seven perfectly matched layers (PML) is used for this simulation. The terminating resistors of  $100\ \Omega$  are placed between each arm ends and the reflector as shown in Fig. 9 and Fig. 10. Fig. 11 shows the plot of return loss with respect to frequency for IRAs with different feed.



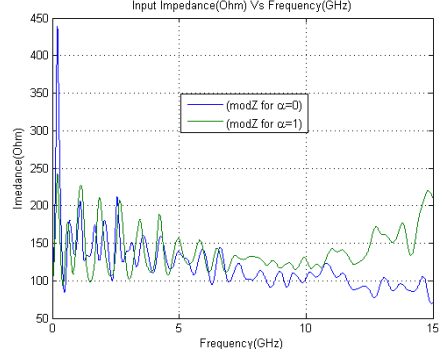
**Figure 9.** Solid geometry of ACD fed ( $\alpha = 0$ ) IRA.



**Figure 10.** Solid geometry of ACD fed ( $\alpha = 1$ ) IRA.



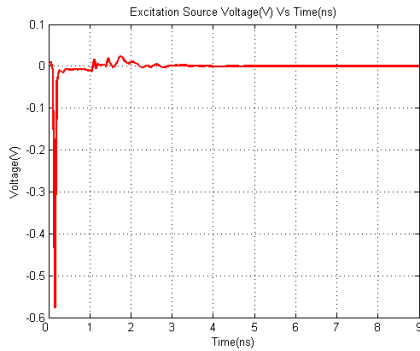
**Figure 11.** Simulated Return loss of ACD fed IRA ( $\alpha = 0$  & 1).



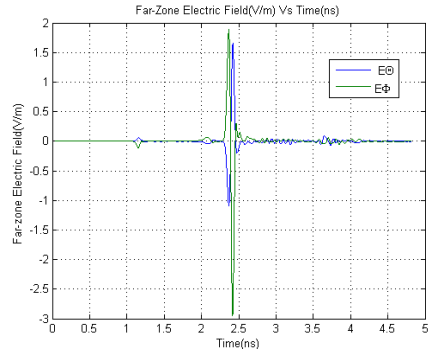
**Figure 12.** Simulated Input Impedance of ACD fed IRA ( $\alpha = 0$  & 1).

Fig. 11 shows that ACD fed IRA ( $\alpha = 1$ ) has better matching at lower frequencies than ACD fed IRA ( $\alpha = 0$ ) because of reduced inductance of the  $\alpha = 1$  profile. The return loss of the antenna with feed profile  $\alpha = 0$  is better than  $\alpha = 1$  at higher frequencies. The input impedance with respect to frequency is shown in Fig. 12 for IRAs with both feed profiles.

The time domain far-zone electric field both  $E_{\Theta}$  and  $E_{\phi}$  (calculated using the excitation signal shown in Fig. 13 at bore-sight of the ACD fed IRAs) consists of prepulse, main impulse and post pulse and is shown in Fig. 14. Fig. 15 shows the time domain far zone response at bore sight for both IRAs. XFDTD (v7.1) solver calculates the far zone electric field at infinity and normalize it to  $|r| = 1$  m. The time domain response of ACD-fed ( $\alpha = 1$ ) is better particularly in late time region but the peak electric field at the bore sight for ACD fed ( $\alpha = 0$ ) IRA is higher than ACD fed ( $\alpha = 1$ ) IRA. The temporal separation observed in the far zone time domain response of the two antennas are due the axial offset of feed arms of ACD fed ( $\alpha = 1$ ) IRA. The gain at bore sight of the ACD fed IRA ( $\alpha = 0$ ) is more than 3dB higher compared to ACD fed IRA ( $\alpha = 1$ ) at high frequencies as shown in Fig. 16. ACD fed IRA ( $\alpha = 0$ ) is considered as a favorable choice for fabrication due to higher gain and comparable time domain performance.



**Figure 13.** Excitation impulse signal used for FDTD analysis.



**Figure 14.** Far-zone electric field of ACD fed ( $\alpha = 0$ ) IRA.

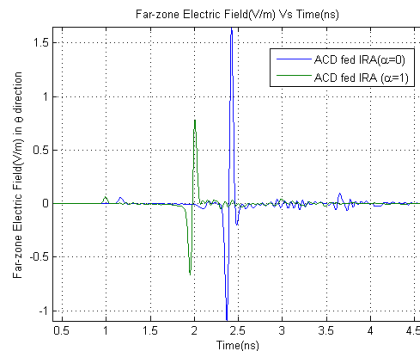


**Figure 15.** Far-zone electric field of ACD fed IRAs ( $\alpha = 0$  & 1).

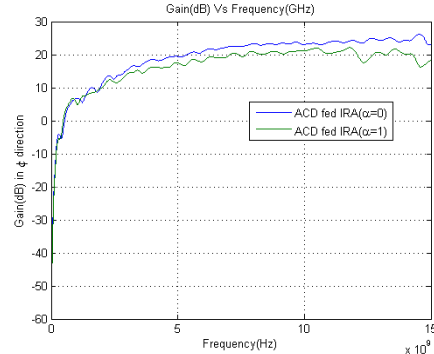


**Figure 16.** Gain of ACD fed IRAs ( $\alpha = 0$  & 1) at bore sight.

#### 4. EXPERIMENTAL RESULTS

FDTD analysis results show that ACD feed ( $\alpha = 0$ ) profile geometry is ideal for ACD fed reflector IRA. For exciting the designed  $100\ \Omega$  antenna, either a balun or a differential converter is required. A balun transforms the antenna impedance achieving compatibility with measuring instruments having a  $50\ \Omega$  impedance. To achieve the same compatibility, a differential converter converts the single ended line to two equal and opposite polarity lines. Therefore, designed antenna was reduced to a half reflector with two arms and a ground plane known as ACD fed half IRA (HIRA). This gave nearly a  $50\ \Omega$  impedance across the requisite frequency range. The realized ACD-fed ( $\alpha = 0$ ) HIRA

is shown in Fig. 17. And its design parameters are given in Table 1. Return loss of the realized HIRA was measured using agilent PNA E8362B Network analyzer. Return loss versus frequency plot (shown in Fig. 18) shows that return loss is better than  $-10$  dB in the frequency range of 500 MHz to 15 GHz. Measured gain of the ACD fed IRA at some of the spot frequencies in the frequency range of 1–15 GHz is shown in Fig. 19.

Radiation pattern of the antenna is measured at ten different frequencies from 1 GHz to 10 GHz in a near field measurement facility. Fig. 20 shows the measured radiation pattern at 2 GHz, 3 GHz, 7 GHz and 10 GHz. The newly developed ACD-fed ( $\alpha = 0$ ) HIRA is



**Figure 17.** Realized ACD fed ( $\alpha = 0$ ) HIRA.

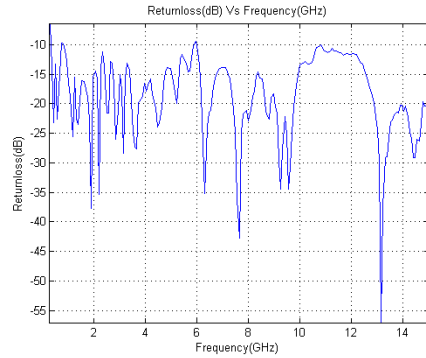


**Figure 18.** Measured return loss of ACD-fed ( $\alpha = 0$ ) HIRA.

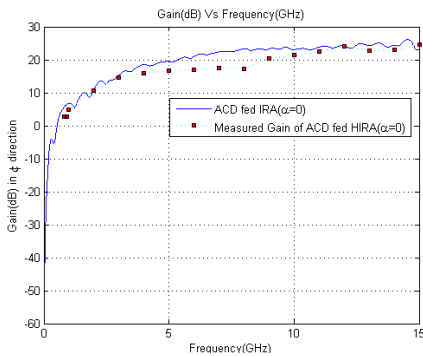


**Figure 19.** Measured gain of ACD fed ( $\alpha = 0$ ) HIRA.

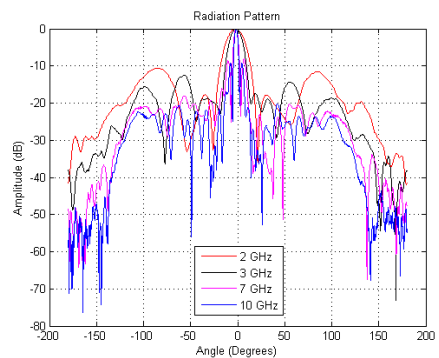


**Figure 20.** Measured radiation pattern of ACD-fed ( $\alpha = 0$ ) HIRA.

**Table 1.** Antenna parameters.

Parameter	ACD feed ( $\alpha = 0$ ) full IRA	ACD-fed ( $\alpha = 0$ ) HIRA	Prototype IRA [11]	Jolt [11]
Reflector diameter D	0.46 m	0.46 m	3.66 m	3.048 m
Focal length F	184 mm	184 mm	1.22 m	1.158 m
F/D	0.4	0.4	0.33	0.375
Number of arms	4	2	4	2
Arm separation	60°	60°	90°	90°
Input impedance ( $\Omega$ )	100	50	200	100
Geometrical factor ( $f_g$ )	0.265	0.132	0.531	0.265
Peak voltage ( $V_p$ )	~ 0.58 volts	0.36 volts	~ 120 kV	890 kV
Max. rate of rise	~ 50 ps	~ 50 ps	~ 100 ps	~ 180 ps
$V_{far}$	~ 7.5 volts	~ 2.4 volts	~ 1280 kV	~ 5.4 MV
Gain ( $G_p$ )	~ 564	~ 71	~ 2230	~ 97
$G_p$ (dB)	~ 27.5 dB	~ 18.5 dB	~ 33.4	~ 20 dB
$E_p(r)$	~ 5.5 V/m at 1 m (Calculation as Eq. (9))	~ 1.41 V/m at 1.65 m (Calculation as Eq. (9))	4.2 kV/m at 304 m [14]	60 kV/m at 85 m [14]
	~ 3 V/m at 1 m (Simulation)	~ 2.4 V/m at 1.65 m (Measured)		

compatible with all the standard instruments as it has nearly  $50\Omega$  impedance across the required frequency range. The time domain response of Novel-fed ( $\alpha = 0$ ) HIRA is measured using measurement setup consists of an UWB arbitrary wave generator (AWG) (Tektronix AWG 7122C), an Oscilloscope (Tektronix TDS71604 DPO 16 GHz), ACD sensor (prodyn AD-70D) and balun (prodyn BIB-100F) as shown in Fig. 21. The differential output of ACD sensor goes to Oscilloscope through the balun which converts it to single ended with a loss of ~ 8 dB. The sensor output after accounting for the balun loss is used

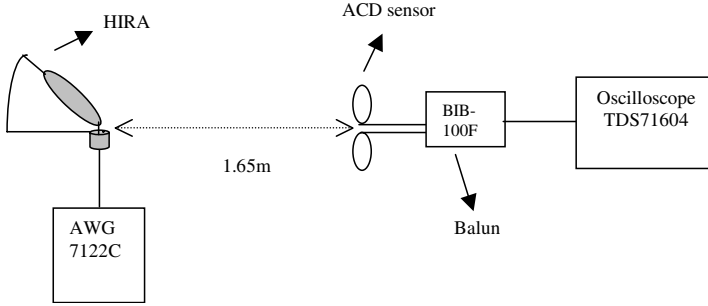


**Figure 21.** Time domain measurement setup.

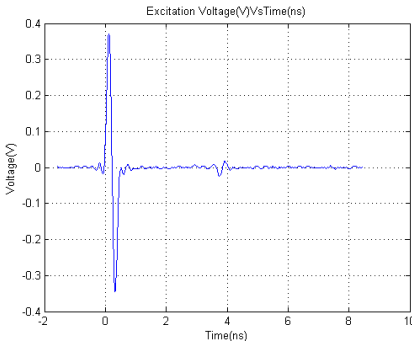


**Figure 22.** Excitation signal used for time domain measurement.

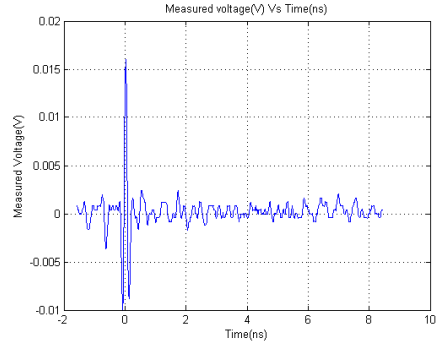


**Figure 23.** Measured time domain response of ACD-fed ( $\alpha = 0$ ) HIRA.

in the Eq. (8) to obtain peak electric field. The input excitation pulse used for antenna evaluation is a gaussian derivative pulse as shown in Fig. 22. The measured time domain response of the ACD-fed HIRA is first time derivative of the input excitation pulse as shown in Fig. 23. The ringing noticed in the antenna response is attributed to the cable pickups.

$$V_0(t) = \vec{A}_e R_0 \varepsilon \frac{\Delta E}{\Delta t} \quad (9)$$

where  $\vec{A}_e = 1 \times 10^{-3} \text{ m}^2 =$  equivalent area of sensor,  $R_0 = 100 \Omega =$  input resistance of sensor,  $V_0(t) =$  Sensor output.

The simplified analytical expressions for peak electric field  $E_p(r)$ , peak gain  $G_p$  and  $V_{far}$  at bore sight of the antenna derived for classical IRA [11] is given in Eqs. (9)–(11) respectively. These expressions are used to calculate the stated parameters for ACD feed ( $\alpha = 0$ ) IRA

and ACD-fed ( $\alpha = 0$ ) HIRA, though they are derived for IRA with triangular feeding plates separated by  $90^\circ$ . Antenna parameters for ACD feed ( $\alpha = 0$ ) IRA and ACD-fed ( $\alpha = 0$ ) HIRA, prototype IRA and Jolt [11] is summarized in Table 1. for reference.

$$E_p(r) = \frac{h_a}{2\pi r c f_g} \left( \frac{dV(t)}{dt} \right) \text{ (V/m)} \quad (10)$$

$$G_p = \frac{1}{\pi f_g} \left( \frac{h_a}{ct_{mr}} \right)^2 \quad (11)$$

$$V_{far} = rE_p(r) \text{ (v)} \quad (12)$$

where,  $h_a$  = equivalent height of antenna,  $f_g$  = geometrical factor,  $V(t)$  = Excitation voltage,  $t_{mr}$  = max. rate of rise,  $c$  = speed of light.

The XFDTD solver gives far zone electric field at a distance of 1 m, therefore analytical (Eq. (9)) and numerical (FDTD) calculation of peak electric field  $E_p$  for ACD feed ( $\alpha = 0$ ) full IRA is done at 1m distance from the antenna. Measurement of electric field for ACD-fed ( $\alpha = 0$ ) HIRA is done at 1.65 m from the antenna. The AWG used as source, generates peak pulse voltage of 0.36 v and the sensor used for measurement has very less sensitivity hence the distance for measurement was restricted to 1.65 m. The peak gain in frequency domain for ACD feed ( $\alpha = 0$ ) full IRA and ACD-fed ( $\alpha = 0$ ) HIRA is in close agreement with their peak time domain gain calculated using Eq. (10). It is difficult to compare the results obtained with classical IRA's because most of them are built with different dimensions, feed configurations and excitation sources [11].

## 5. DISCUSSION

ACD is used as a sensor for measuring fast electromagnetic pulse [9]. An attempt is made here to find out ideal profile of ACD antenna, which can be used as a feed for reflector IRA. The analysis results shows that ACD antennas with  $\alpha > 0$  has better time domain response and good low frequency performance. As the ratio of point charge to line charge density ( $\alpha$ ) increases the girth of the ACD feed also increases, increasing the feed blockage of the antenna. Hence as an asymptotic conical dipole antenna, higher value of  $\alpha$  is good but ACD used as a feed for reflector IRA,  $\alpha = 0$  (only linear charge density) is ideal charge distribution used to generate ideal ACD profile. This ACD profile used as feed allows achieving smaller impedance value with smaller cone angle and smaller form factor. The ACD fed HIRA realized using the ideal profile is readily used with single-ended  $50 \Omega$  pulse generators and other measurement instrumentation.

## 6. CONCLUSION

The point charges used in the equivalent charge method improves the time domain response, particularly in late time because of reduced inductance. The increase in the girth of the dipole for the profiles with  $\alpha > 0$  increases the feed blockage and hence  $\alpha = 0$  is ideal ACD feed profile. The measured results of the ACD-fed HIRA show the suitability of novel feed for reflector IRAs.

## REFERENCES

1. DuHamel, R. H., et al., "Frequency independent conical feeds for lens and reflectors," *Proc. IEEE Int. Antennas Propagation Symp. Dig.*, Vol. 6, 414–418, Sep. 1968.
2. Baum, C. E., "Radiation of impulse-like transient fields," Sensor and Simulation Note #321, Nov. 25, 1989.
3. Baum, C. E. and E. G. Farr, "Impulse radiating antennas," *Ultra-wideband Short Pulse Electromagnetics*, H. L. Bertoni, et al., Eds., 139–147, Plenum Press, NY, 1993.
4. Baum, C. E., "Configuration of TEM feed for IRA," Sensor and Simulation Note 327, Apr. 27, 1991.
5. Farr, E., "Optimizing the feed impedance of impulse radiating antenna, Part I: Reflector IRA," Sensor and Simulation Notes 354, Jan. 1993.
6. Farr, E., "Development of a reflector IRA and a solid dielectric lens IRA," Sensor and Simulation Note 396, Apr. 1996.
7. Manteghi, M. and Y. Rahamat-Sammii, "A novel Vivaldi fed reflector impulse radiating antenna (IRA)," *Proc. IEEE Int. Symp. Antennas and Propagation*, 549–552, Washington, DC, Jul. 3–8, 2005.
8. Manteghi, M. and Y. Rahamat-Sammii, "On the characterization of a reflector impulse radiating antenna (IRA): Full-wave analysis and measurement results," *IEEE Trans. Antennas and Propagation*, Vol. 54, No. 3, 812–822, Mar. 2006.
9. Baum, C. E., et al., "Sensors for electromagnetic pulse measurements both inside and away from nuclear source regions," *IEEE Trans. Antennas and Propagation*, Vol. 26, 22–35, Jan. 1978.
10. Bowen, L. H., et al., "A high voltage Cable feed impulse radiating antenna," *Ultrawideband Short Pulse Electromagnetics*, Baum et al. (eds.), Vol. 8, 9–16, Springer, 2007.

11. Giri, D. V., "Peak power gain in time domain of impulse radiating antenna (IRAs)," *Sensor and Simulation Notes* 546, Oct. 2009.
12. Sower, G. D., "Optimization of the asymptotic conical EMP sensors," *Sensor and Simulation Notes* 295, Oct. 1986.
13. Baum, C. E., "An equivalent charge method for defining geometries of dipole antennas," *Sensor and Simulation Notes* 72, Jan. 1969.
14. Giri, D. V., *High-power Electromagnetic Radiators*, Harvard University Press, 2004.
15. Singh, D. K., D. C. Pande, and A. Bhattacharya, "A new feed for reflector based  $100\Omega$  impulse radiating antenna," *PIERS Proceedings*, 1635–1639, Kuala Lumpur, Malaysia, Mar. 27–30, 2012.